Chapter 5

Depth imaging passive seismic data

SUMMARY

Migrating the synthesized shot gathers produced in Chapter 2 produces very clear images even when the synthesized gathers look noisy or completely incorrect. Incomplete distribution of subsurface sources surrounding the domain of interest is the most likely weakness in a passive recording campaign. This problem causes coherent noise events in the synthesized gathers that do not conform to the kinematics of the active reflection seismic experiment. Migration minimizes the minimizes the effect of coherent noise in the synthesized gathers and correctly images subsurface structure even when events in the gathers do not appear to conform to the conventional experiment. For this reason, I believe migration should be a near mandatory processing step for transmission wavefields when permissible. Direct migration of raw passive data produces accurate subsurface images without first synthesizing shot gathers. The images produced by direct migration are almost indistinguishable from those produced by migrating the synthesized shot gathers with the synthetic tests presented in Chapter 2. Under most scenarios, direct migration saves substantial computational cost. Any migration strategy that maintains separate upcoming and down-going wavefields and employs a correlation based imaging condition to combine them at depth can be employed to migrate transmission wavefields.

INTRODUCTION

A 5D volume of seismic data is a voluminous and complicated volume to interpret, that doesn't recapitulate humans' 3D concept of space. Offset, moveout, traveltime, interference, and high dimensionality make interpreting the subsurface in the data domain a challenging task. When the data is in the form of transmission wavefields due to unknown sources with incomplete subsurface distribution, the gathers synthesized via correlation may be impossible to interpret correctly. Under scenarios expected to be realistic with field data, shown in Chapter 2, small violations of the assumptions behind correlation processing of transmission wavefields can quickly make the synthesized gathers uninterpretable. This chapter investigates the extent to which the artifacts in the synthesized gathers affect the image space after migration.

Migration is a powerful data processing tool to collapse dimensionality and sum redundant information as a function of offset to subsurface location. Shot-profile depth migration is a powerful, robust algorithm to process active seismic data and return an interpretable subsurface volume. Fortuitously, recapitulating the seismic experiment in the computer during migration can reduce coherent noise events in the data volume that do not comply with the kinematics of simple reflections. Images still suffer from coherent noise, but it is often more recognizable as implausible, and easily ignored or removed. Interpreting a dense 3D image volume is also much easier than a sparse 5D data volume.

In Chapter 2, cross-correlation of transmission wavefields was analyzed in terms of its efficacy in synthesizing shot gathers from a conventional surface seismic active survey. In this chapter, I present depth images produced with shot-profile migration using the correlation volumes shown previously. The best synthesized volume of data was produced by summing the correlations from the transmission wavefields from 225 impulsive sources across the bottom of the model domain. This volume still contains many artifacts. Progressively poorer correlation volumes were produced by using very few of the transmission wavefields and by correlating the sum of transmission wavefields. The first section of this chapter presents the images produced by migrating those synthesized gathers.

Next, I develop the processing of passive seismic data as a migration operation: direct migration. Artman and Shragge (2003) introduced the applicability of direct migration for

transmission wavefields. Artman et al. (2004) provided the mathematical justification for zero-phase source functions. Shragge et al. (2006) showed results for the special case of imaging with teleseismic events. Direct migration of transmission wavefields requires an imaging algorithm composed of wavefield extrapolation and a correlation based imaging condition. Shot-profile wave-equation depth migration (Claerbout, 1971) fulfills these requirements. Images produced by direct migration are presented to show the validity of the new method.

MIGRATION OF SYNTHESIZED GATHERS

The first two panels in Figure 5.1 are two shot gathers from the volume of synthesized gathers produced by summing the correlations calculated from all 225 transmission wavefields as described in Chapter 2. The virtual shot locations for the gathers are indicated by vertical lines. The right panel is the zero-subsurface offset image produced by shot-profile migration of the entire volume from which the gathers were extracted. All images produced in this chapter are zero-subsurface offset images. The delta function in equation 1.3 results in a strong flat event at $z = 0$ m in the image. To diminish that event and boost the amplitude of the second reflector, the image was processed with a depth-dependent gain function. All images in this chapter are presented with this same post-processing step. The event that partially obscures the second reflection is the first order multiple between the surface and the first reflector. Despite the imperfections in the synthesized gathers compared to active surface seismic gathers, the resulting image is very clear. Because most of the noise events in the synthesized gather do not conform to the kinematics of the reflection experiment from which the migration algorithm is designed, their effects are minimal in the image domain.

The left column of Figure 5.2, panels `a` and `c`, are correlated gathers from a single source beneath the left edge of the model domain whose generation was explained in Chapter 2. The right column, panels `b` and `d`, shows active data modeled at the same shot locations. The correlated gathers suffer many problems that make them obviously poor reproductions of the surface data modeled to the right. The gathers are a partial result of the summation over subsurface source required by the development of correlation processing to synthesize active surface data. The synthesized gathers are not just poor quality, but produce completely wrong

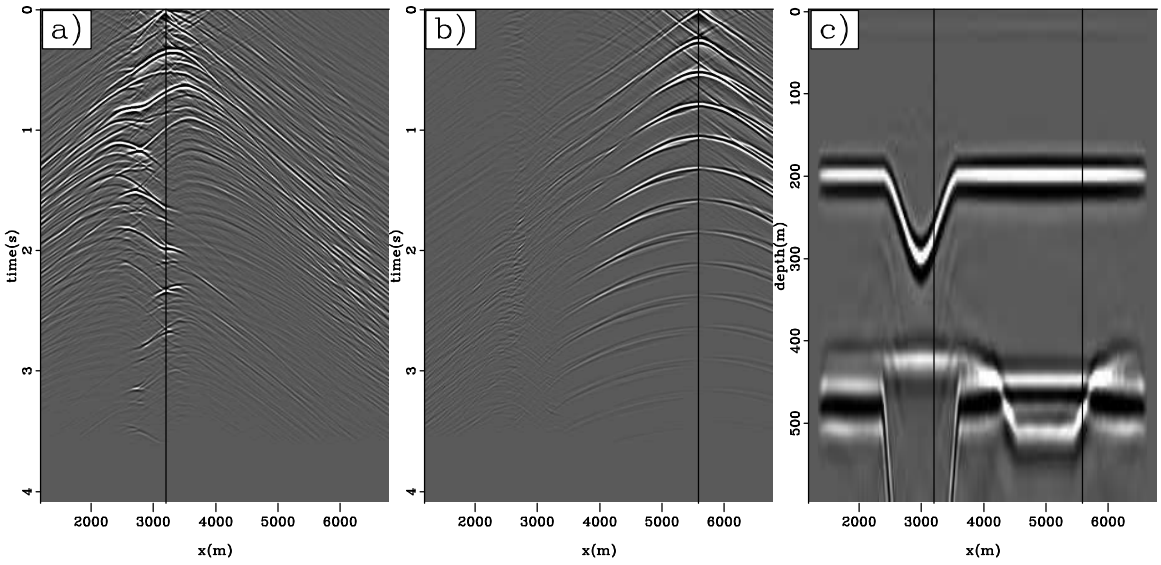

Figure 5.1: Representative gathers synthesized by summing correlations from all modeled transmission wavefields (zero-offset trace under black line) and the depth image produced with shot profile migration of all such gathers. DepthSyn-mig.all [CR]

kinematics at far offset. Most of the energy in panel c is from the high order multiples in the transmission wavefield. There is seemingly no correspondence between the panels c and d.

Figure 5.3 shows two images produced from the volume of synthesized gathers using a transmission wavefield due to a single source beneath the left edge of the model (left column Figure 5.2). Panel a is the migration of all gathers produced by correlation. Structure on the right side of the model and down-right dipping structure is diffuse and weak. However, the entire domain is correctly imaged. Panel b was produced by migrating the synthesized shot gathers from only the right side of the model (such as Figure 5.2c). Without the strong, well-imaged left side of the domain, the gain for the figure is substantially boosted which shows more of the background noise. However, the noise is not coherent, and the power of events is substantially above the noise level. The negative (black) part of the wavelet below the reflector is lost, but the positive (white) peak is in the same location ($z = 200$ m) as in the left panel. Despite the correlated gathers on this half of the domain looking completely incorrect (bottom Figure 5.2), using them as data for migration has correctly imaged the subsurface structure.

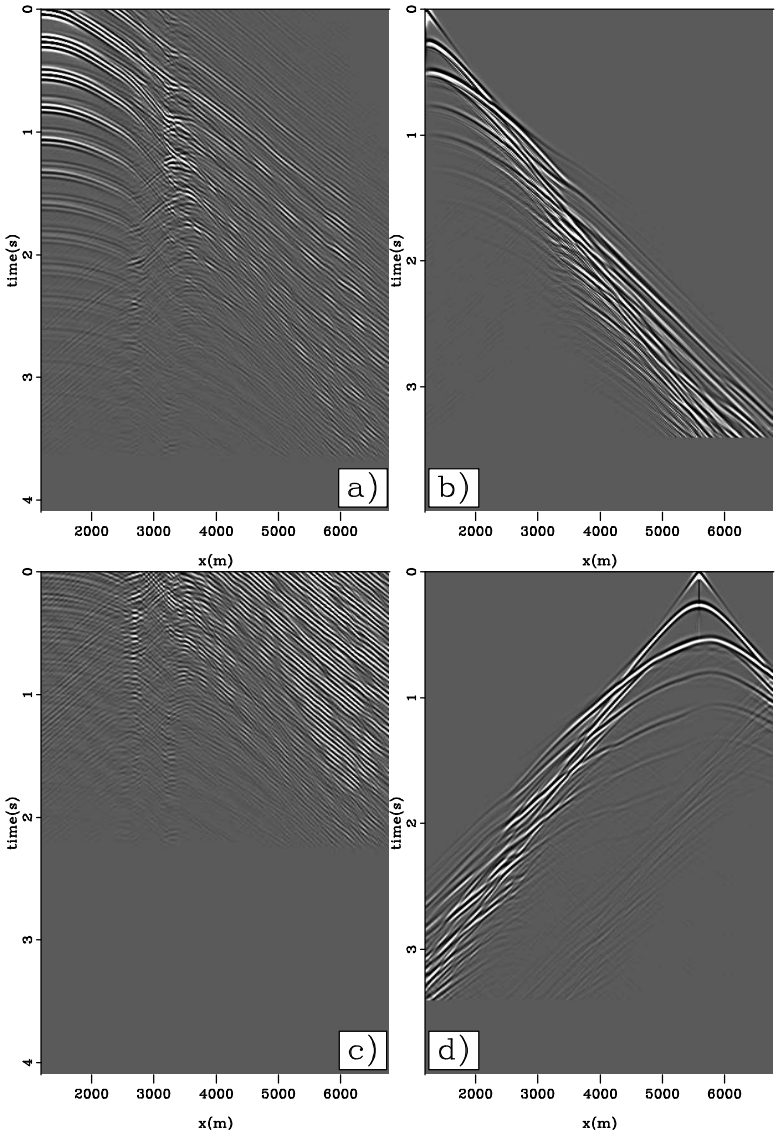

Figure 5.2: Left column: Synthesized gathers from left and middle of synthesized data volume produced with a single transmission wavefield due to a source below the left edge of the model domain. Right column: active surface data at the same (virtual) shot locations. DepthSyn-dat1200 [CR]

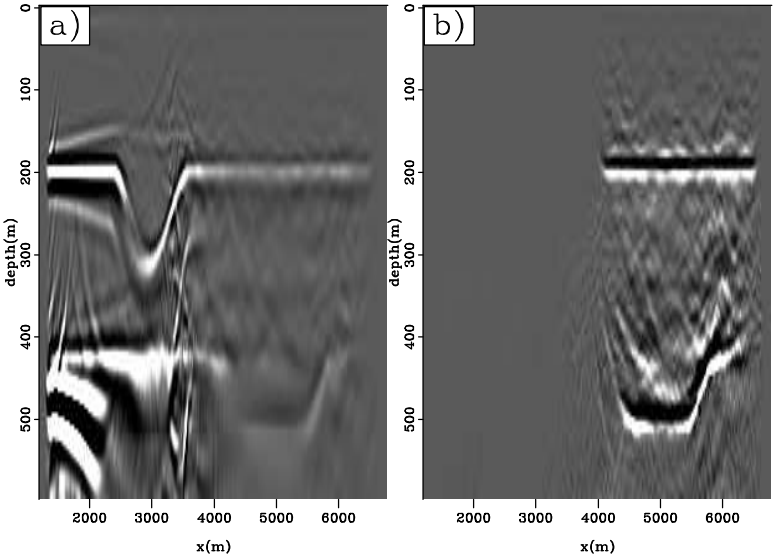

Figure 5.3: a) Image produced by migrating all synthesized gathers from a single transmission wavefield due to an impulsive source at the left edge of the domain. b) Image produce by migrating right half of the total volume of synthesized gathers. DepthSyn-mig.shot1200 [CR]

Figure 5.4 presents a suite of migrations using the correlation volumes produced in the previous chapter generated to explore the possible deleterious effects of processing two transmission wavefields simultaneously. The synthesized gathers presented previously were obscured by the superposition of two correlation results. The gathers were not uninterpretable, but without knowing that two sources were contained within the transmission wavefield, it is likely that the subsurface would be misinterpreted. The structure revealed in these depth images however is very easy to accurately interpret and noise is easily identified as such. The top row are images produced by migrating the correlations of summed transmission wavefields. The left panel used impulsive wavefields, and the right panel used randomized wavelets. The same is true for the bottom row of images, which show the migration of summed correlation volumes from the two wavefields. The bottom row thus represents a correctly processed partial result (independent correlation).

Despite the fact that the model was illuminated with only two subsurface sources, all the structure is well imaged in Figure 5.4. Much of the noise in the panel a is eliminated in panel c by correctly processing the transmission wavefields one at a time. The images in the right column are almost identical. In fact, migrating the correlations from the transmission wavefield modeled due to a single source below the middle of the model domain produces a similar image. Figure 2.8 shows that the random wavelet used for the source at the left edge

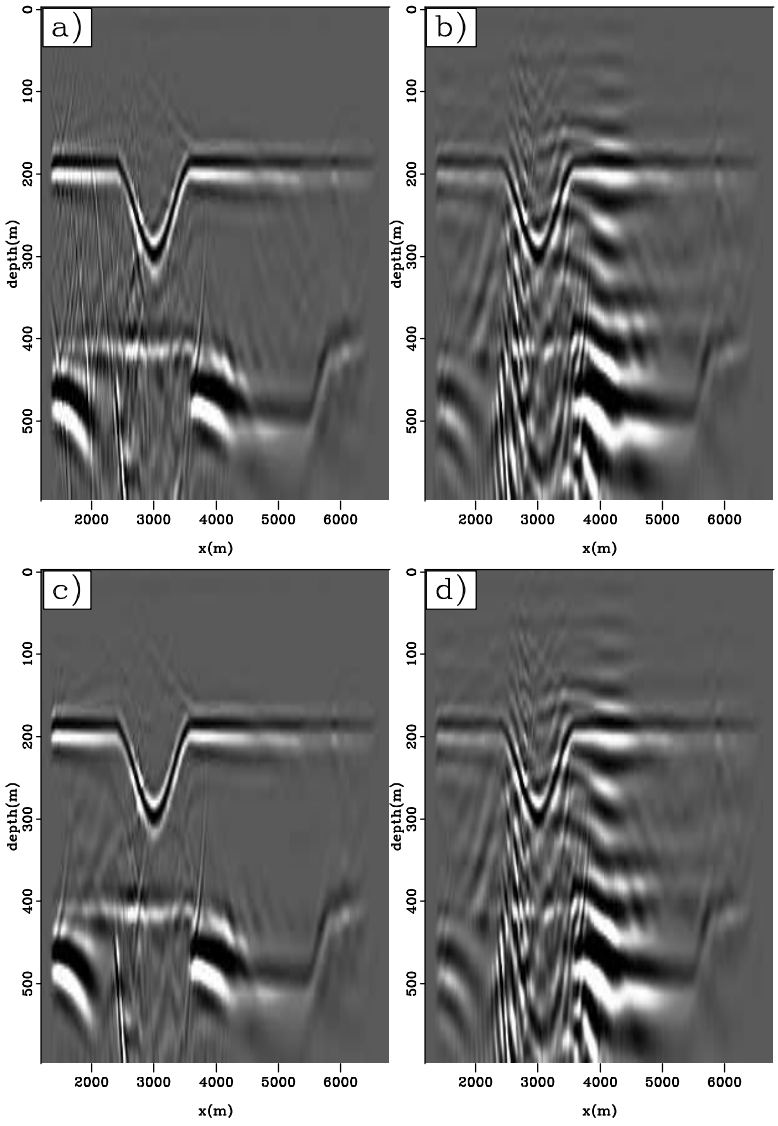

Figure 5.4: Images obtained from migrating correlation volumes due to two sources (located below the left edge and center of model domain). Left column used impulsive sources, while source functions were randomized for the right column. Top row was produced with summed transmission wavefields, while bottom row from sum of correlations of transmission wavefields. DepthSyn-mig.shot1200.3500 [CR]

of the model also contains a nearly 2 s time delay. Therefore, this energy is not included in the image at such shallow depths.

Figure 5.5 shows images produced by migrating the correlations produced with wavefields that contain more than two subsurface sources. The top row was produced with the synthesized correlations from the sum of 25 transmission wavefields due to sources evenly distributed across the bottom of the model domain. The bottom row was produced with 30 sources located around the center of the model domain. The sources in the left column were all impulsive. The right column was produced by first adding a random phase shift and wavelet coda to each transmission wavefield before summing.

The top row of images in Figure 5.5 fully illuminate the structure, though steeply-dipping noise-trains are seen due to the sparse sampling of subsurface sources and the correlational interference of all the individual wavefields. Similar features are in visible in Figure 5.4a. The addition of randomized wavelets in panel b does not substantially differentiate the result from the image in panel a. The noise events are less structured, but there are some flat semi-coherent events between the reflectors, and the second reflector is marginally less continuous.

The bottom row of images in Figure 5.5 have less artifacts than the images above them, but do not illuminate the structure as well due to the limited distribution of subsurface sources. Since the subsurface sources used were so close together, the events are highly correlatable across the space-axis near the flat hyperbola tops in the raw data. This leads to the strong, low frequency noise in the center of the images. A low-cut filter can remove this energy to provide better imaging of the second reflector, but the filter cut-off must be carefully chosen since the frequency content of the noise events is only marginally below that of the real reflectors. The randomized wavelets introduced to the input for the image in panel d remove much of the low frequency noise in the center of panel c. The noise is less structured, and the overall quality of the image is improved.

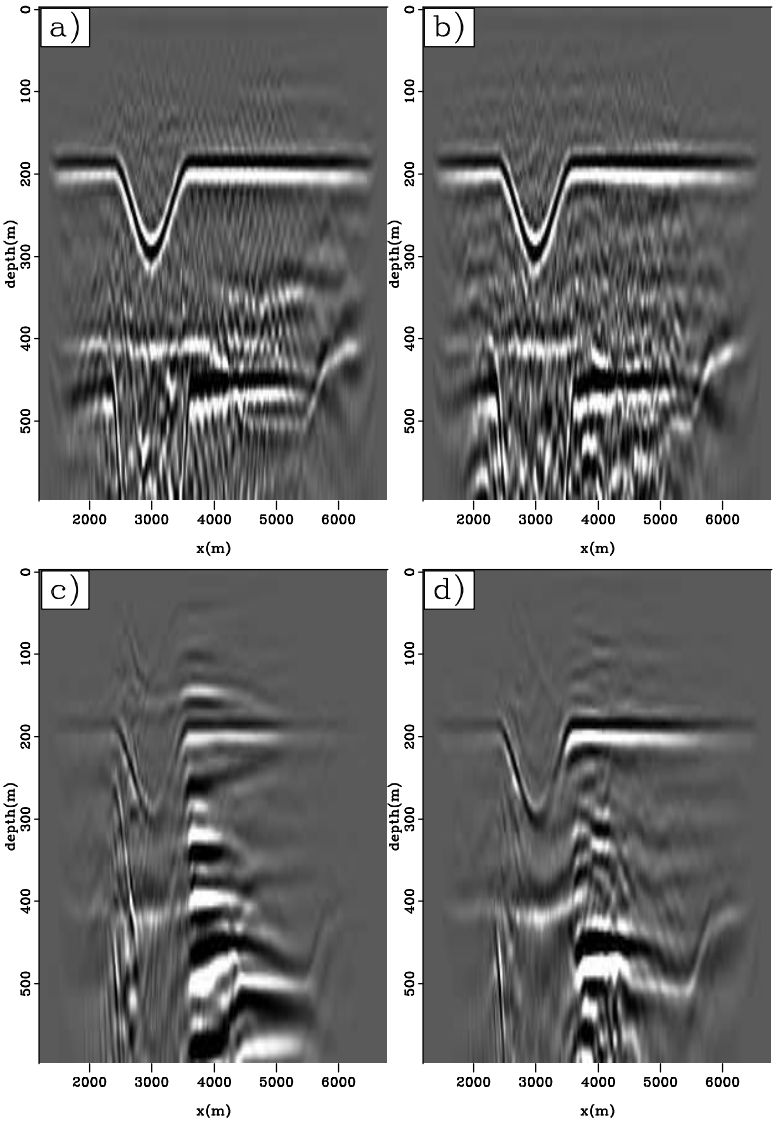

Figure 5.5: Images produced by migrating synthesized gathers of the summed transmission wavefields from many sources. Top row: Migrations of correlations from the sum of 25 transmission wavefields due to sources across the bottom of the model domain. Bottom row: Migrations of correlations from the sum of 30 transmission wavefields due to sources clustered around the center of of the model domain. Left column used modeled wavefields while right column was produced after introducing randomized source functions. DepthSyn-mig.shotsmall [CR]

DIRECT MIGRATION

Theory

Shot-profile migration uses one-way extrapolators to independently extrapolate up-going, U, and down-going, D, energy through the subsurface velocity model. U, extrapolated acausally, is a single shot gather. D, extrapolated causally, is a wavefield modeled to mimic the source used in the experiment. I will define the causal extrapolation operator, E^+, and the acausal operator, E^-. These one-way operators can not extrapolate evanescent or overturning waves, but this limitation is not crippling when subsurface reflectors are not very steep. In this thesis, I use the split-step Fourier plus interpolation (SSF-PI) (Kessinger, 1992) for all migration operations.

Wavefields are extrapolated to progressively deeper levels, z, by recursive application of $E^{\pm}$

$$U_{z+1}(\mathbf{k}_x;\mathbf{x}_s,\omega) = E^- U_z(\mathbf{k}_x;\mathbf{x}_s,\omega) \tag{5.1}$$

$$D_{z+1}(\mathbf{k}_x;\mathbf{x}_s,\omega) = E^+ D_z(\mathbf{k}_x;\mathbf{x}_s,\omega). \tag{5.2}$$

With two wavefields at each depth, an imaging condition is invoked to extract energy for the image, i, that is collocated within the two wavefields. The zero-offset imaging condition for shot-profile migration is defined as the zero lag of the cross-correlation of the two wavefields

$$i_z(\mathbf{x}) = \sum_{\mathbf{x}_s}\sum_{\omega} U_z(\mathbf{x};\mathbf{x}_s,\omega) D_z^*(\mathbf{x};\mathbf{x}_s,\omega)\,. \tag{5.3}$$

The sum over frequency extracts the zero lag of the correlation. The sum over shots, $\mathbf{x}_s$, stacks the overlapping images from all the individual shot gathers.

The important implication of the shot profile strategy is that the causal and acausal extrapolation operators applied to the down-going and up-coming energy are applied to orthogonal components of the seismic experiment. This is the reason that two one-way operators can be

used in place of two-way operators to recapitulate the seismic experiment in the computer.

Transmission wavefields are defined as the superposition of the up-coming and down-going seismic energy. As such, the down-going energy defined above as D and the up-coming energy, U, are both contained within the data. Therefore, propagating a transmission wavefield causally will correctly extrapolate the down-going energy contained therein for migration. Similarly, propagating a transmission wavefield acausally will correctly extrapolate the up-coming energy for migration. The correlation applied in the imaging condition, equation 5.3, performs the trace comparison required to synthesize active data from transmission data. Performing this operation in the image space simply moves the correlation processing into the subsurface from the acquisition plane. This result is proved in terms of a redatuming experiment in Artman et al. (2004), and independently derived by Borcea et al. (2003).

The phase-encoding framework explained in Chapter 1 was developed originally as a migration algorithm. Recognizing the similarities between a transmission wavefield and a phase-encoded wavefield naturally leads to direct migration. Instead of convolving the gathers with a synthetic encoding function and summing across the shot axis, we can view a transmission wavefield as the sum of shot gathers convolved with a subsurface source function (and all surface-related and internal multiples). Therefore, the Earth provides the encoding function, and we can migrate the encoded wavefield to produce a subsurface image. The principle difference between the phase-encoded sum of all shots and and a transmission wavefield, is that the transmission wavefield is defined, in equation 1.3, as a function of a single subsurface source, ξ. Therefore we must sum the images produced from each transmission wavefield due to sources ξ to build full illumination and cancel artifacts, just as the the correlations are summed when integrating over source ξ in equation 1.3.

The source wavefield, $\hat{S}$, required to migrate phase encoded gathers (or transmission wavefields) was presented in equation 1.1 as the sum of all the encoding functions with which the gathers were convolved. The transmission wavefield contains this sum and many more events. However, just as inappropriate events in synthesized gathers produced with individual transmission wavefields are destroyed through destructive interference during summation, the cross-talk events in direct migration images are eliminated by summing the images from individual transmission wavefields.

shot-profile migration				transmission imaging		
$U_{z=0}(\mathbf{x};\mathbf{x}_s,\omega)$	$\otimes$	$D_{z=0}(\mathbf{x};\mathbf{x}_s,\omega)$	$=$	$T_{z=0}(\mathbf{x};\xi,\omega)$	$\otimes$	$T_{z=0}(\mathbf{x};\xi,\omega)$
$\vert$		$\vert$		$\vert$		$\vert$
E^-		E^+		E^-		E^+
$\downarrow$		$\downarrow$		$\downarrow$		$\downarrow$
$U_{z=1}(\mathbf{x};\mathbf{x}_s,\omega)$	$\otimes$	$D_{z=1}(\mathbf{x};\mathbf{x}_s,\omega)$	$=$	$T^-_{z=1}(\mathbf{x};\xi,\omega)$	$\otimes$	$T^+_{z=1}(\mathbf{x};\xi,\omega)$

Table 5.1: Equivalence of shot-profile migration of reflection data and direct migration of transmission wavefields, $T(\mathbf{x},\xi,t)$. $\mathbf{x}_s$ has a similar meaning to ξ. $\sum_{\mathbf{x}_s,\xi}$ and $\sum_\omega$ produces the image $i_z(\mathbf{x})$ for both methods. Only first and second levels of the recursive process are depicted.

The physics captured in the formulation of shot-profile migration remains the same regardless of the temporal or areal characteristics of the initial conditions in the wavefields. The data records provide boundary conditions for the experiment migration attempts to reverse in the computer. The extraction of only the zero lag of the correlation for the image discards energy in the two wavefields that is not collocated. This includes much of the energy that has been extrapolated in the wrong direction (since the same data is used initially for both U and D wavefields). However, some cross-talk will be introduced since this approach strictly violates the phase-encoded migrations strategy described in Chapter 1.

Table 5.1 pictorially demonstrates how direct migration of transmission wavefields fits into the framework of shot-profile migration to produce the 0^{th} and 1^{st} depth levels of the zero-offset image. The correlation in the imaging condition takes the place of the correlation in equation 1.3 to synthesize shot gathers. The summations over shot locations and frequency in equation 5.3 are omitted to reduce complexity. Note however, that the sum over shot locations in equation 5.3 takes the place of the integral over subsurface sources in equation 1.3. Also, after the first extrapolation step, using the two different phase-shift operators, the two transmission wavefields are no longer identical, and can be redefined U and D. This is noted with superscripts on the T wavefields at depth. Synthesizing shot gathers by correlation followed by migration is represented by movement from the top-right of the table to the conventional data domain on the left, and then down via conventional migration.

When considering the case of direct migration of transmission wavefields due to multiple sources, a summation over ξ is implied in field data used as data on the right column of Table 5.1. This can happen when subsurface sources are not well separated in time, or are too weak to be apparent in the raw data to facilitate separation by time windowing. If we assume that we can not separate passive records into individual transmission wavefields, field data, T_f, is most likely a partial sum over subsurface source

$$T_f(\mathbf{x},\omega) = \sum_{\xi}^{n} T(\mathbf{x},\xi,\omega)\,, \tag{5.4}$$

where n is an unknown number of sources that were active during the recording of the passive data. Processing relatively short time windows independently will tend to minimize n, though can not address the possibility that multiple sources may be firing simultaneously as can be expected if the ambient sonic energy is caused by cultural noise or reservoir compaction, for example.

Source summation is explicitly included in the conventional migration flow shown on the left column of Table 5.2. The implicit sum over subsurface sources for the transmission wavefields on the right column is indicated by not parameterizing the wavefield as a function of ξ. After summing across the source axis of a conventional reflection seismic data volume, the appropriate source wavefield, the sum of all the impulsive down-going wavefields, is a horizontal plane wave. The direct migration of summed transmission wavefields is very analogous to the horizontal plane-wave migration strategy, though if the number of subsurface sources is small, a complete plane wave will probably not be manufactured. Further, unless the sources fire simultaneously, they will not construct a horizontal plane wave no matter how many are included in the transmission wavefield. In this case, the combined direct arrival of the multiple sources forms an unknown wavefront that provides the source function to be used as the down-going source energy. For this reason, I label the approach wavefront imaging.

Figure 5.6 shows the summation of direct arrivals from multiple subsurface sources that will reflect from the free surface to provide the down-going energy to investigate the subsurface. These are the wavefront source functions to which I am referring with the name "wavefront imaging." Panel a is a single direct arrival from a source below the center of the

plane-wave migration				wavefront imaging		
$\left(\sum_{\mathbf{x}_s} U_{z=0}(\mathbf{x};\mathbf{x}_s,\omega)\right)$	$\otimes$	$\left(\sum_{\mathbf{x}_s} D_{z=0}(\mathbf{x};\mathbf{x}_s,\omega)\right)$	$=$	$T_{z=0}(\mathbf{x},\omega)$	$\otimes$	$T_{z=0}(\mathbf{x},\omega)$
$\vert$		$\vert$		$\vert$		$\vert$
E^-		E^+		E^-		E^+
$\downarrow$		$\downarrow$		$\downarrow$		$\downarrow$
$U_{z=1}(\mathbf{x},\omega)$	$\otimes$	$D_{z=1}(\mathbf{x},\omega)$	$=$	$T^-_{z=1}(\mathbf{x},\omega)$	$\otimes$	$T^+_{z=1}(\mathbf{x},\omega)$

Table 5.2: Equivalence between direct migration of passive field data and simultaneous migration of all shots in a reflection survey. Only first and second levels of the iterative process are depicted. $\sum_\omega$ produces the image i_z for both methods.

model domain. Panel b is the wavefront due to 30 subsurface sources clustered over 600 m beneath the center of the domain. Panel c is the wavefront due to 25 subsurface sources evenly distributed across the entire bottom of the model domain. The direct arrival is actually only a part of the appropriate source wavefield required to image the subsurface. It is the principle component, but multiple events image subsurface reflectors as downgoing energy for the next higher-order multiple in the transmission wavefield extrapolated acausally, as will be shown in Figure 5.7.

Synthetic tests

The modeled transmission wavefields used in previous examples are again used below to produce images with the direct migration strategy presented above. In addition to direct migration, images are also prdduced using the direct arrival from subsurface sources for the down-going source wavefield and horizontal plane-wave migration. Some figures from above are presented again next to their direct migration counterpart to facilitate comparissons between the two approaches.

Figure 5.7 shows images produced with several processing strategies all beginning with the transmission wavefield due to a single impulsive source at the left edge of the model domain. The left panel, direct migration, is much stronger on the left edge of the model. The entire domain is imaged fairly well, and the imperfections are easily identified. Because the right

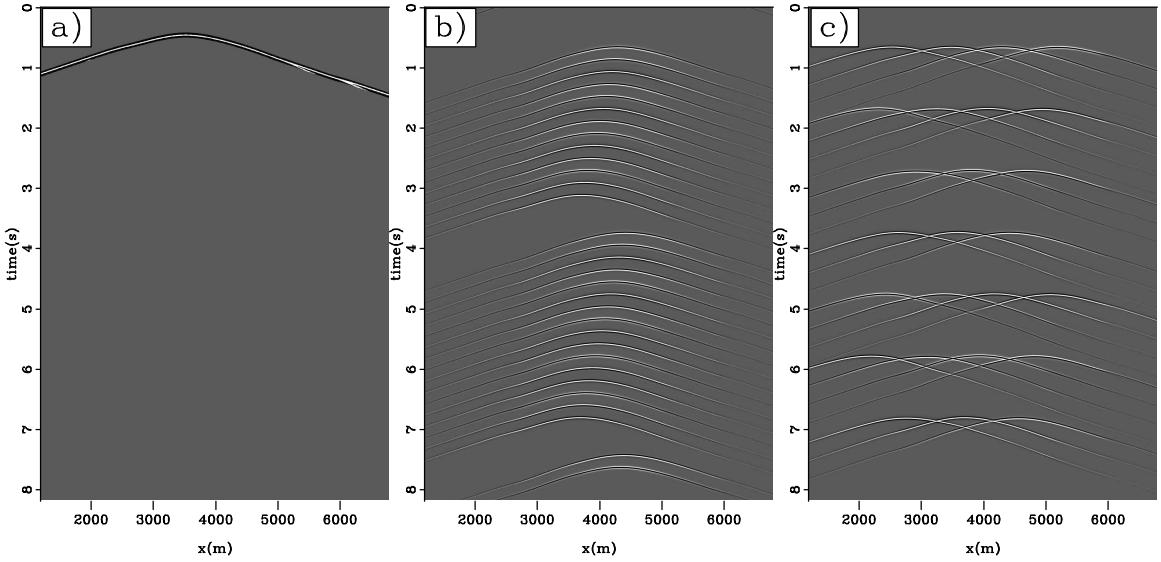

Figure 5.6: a) Direct arrival of energy from a source below the center of the model domain. b) Wavefront due to the sum of direct arrivals from 30 subsurface sources spanning 600 m around the center of the domain. c) Wavefront due to the sum of direct arrivals of 25 subsurface sources evenly distributed across the bottom of the domain. Randomized source functions were used in panels b) and c). DepthSyn-directsum [CR]

side of the domain is so weak however, it is probable that this structure would be below the noise threshold in a field experiment with weak, unidentifiable sources.

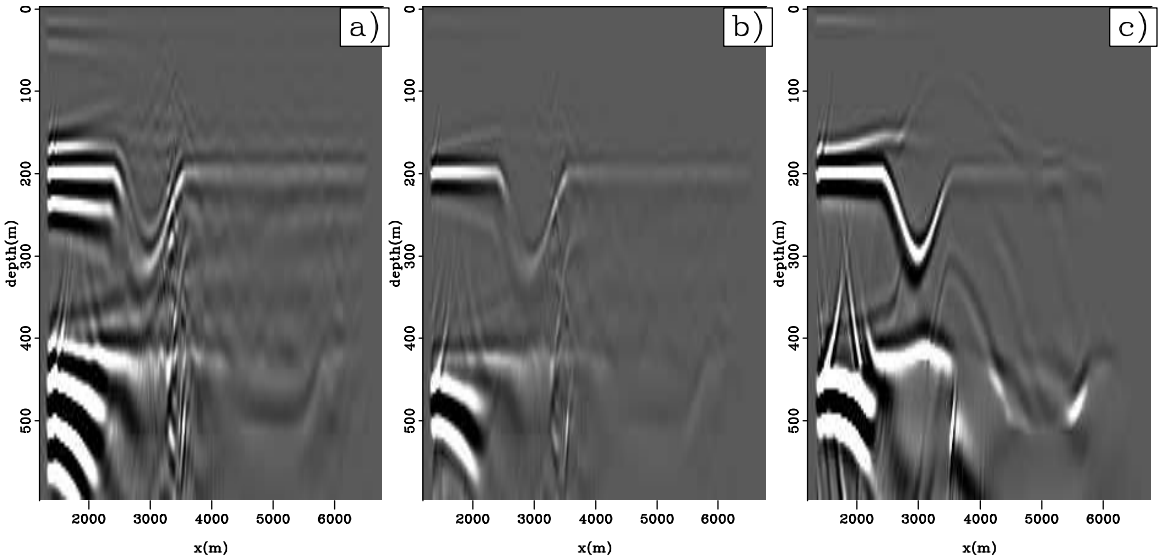

Figure 5.7: a) Direct migration of a transmission wavefield due to an impulsive subsurface source at the left edge of the model domain. b) Migration of synthesized gathers produced with the same transmission wavefield. c) Image produced with transmission wavefield as data and only the direct arrival as the source. DepthSyn-dmig1200 [CR]

Figure 5.7b is the same image shown in Figure 5.3a for comparison to the direct migration result, Figure 5.7a. The migration of the synthesized gathers, b, provides a better image than the direct migration. Both images are incomplete results. The image produced by direct migration of 280 traces is over two orders of magnitude less expensive to produce than migrating the 78,400 traces in the volume of synthesized gathers. This cost difference does not include the further cost incurred by the correlations required to compute the synthesized gathers. In this case, of a single subsurface source near the edge of the domain, direct migration could be used as a convenient data-mining processing step to determine if the additional expense to produce panel b is appropriate.

Figure 5.7c was produced using the same transmission wavefield due to a single subsurface source below the left edge of the domain used for input in panels a and b. This image was

created using the total transmission wavefield for the the up-going (data) wavefield. The down-going (source) wavefield was only the direct arrival from the subsurface source. The image has less cross-talk noise than the left image. However, the right edge of the model and the second reflector are not imaged as well. Recall that the synthesized gathers on the right edge of the domain produced with this transmission wavefield, Figure 5.2c, contain energy from only high-order multiples. Therefore, the appropriate source wavefield for migrating a single transmission wavefield is not simply the direct arrival, but should also include some primary and/or multiple events. Using the entire transmission wavefield as a source function produces cross-talk in an image due to a single transmission wavefield. However, using only the direct arrival as a source function does not fully utilize all of the events in the transmission wavefield.

Figure 5.8 shows images produced with the various migration strategies available when processing a transmission wavefield due to two subsurface sources, one at the left edge and one below the center of the model domain. Panel a shows the direct migration of the sum of the two impulsive transmission wavefields. The result in panel b includes randomized source functions with the same transmission wavefields. Panel c is the sum of the images produced by direct migrations of the two impulsive wavefields. Panel d is the result of migrating the correlations produced with the sum of the two randomized transmission wavefields, Figure 5.4d. The sum of direct migrations, panel c, is clearly the best image, as dictated by theory. The main problem in the image is partial illumination. There is very little difference between the upper two images (with and without randomized wavelets). The comparison between panels b and d shows that there is very little difference between the direct migration (b) and the migration of the synthesized correlations (d). There is a small phase roll between the two images, but the two methods provide roughly equivalent imaging capability.

Figure 5.9 presents images produced with various processing strategies, but always using all 225 transmission wavefields from sources across the entire bottom of the model domain. Panel a was produced by direct migration of the sum of all 225 modeled wavefields. In this case, the minimum traveltime of the direct arrival for each transmission wavefield is constant, and therefore the summation builds a strong horizontal plane wave as a direct arrival. The data for direct migration used to produce the image in panel b and long image in panel e included the addition of randomized source functions. Panel e is the same as panel b with an

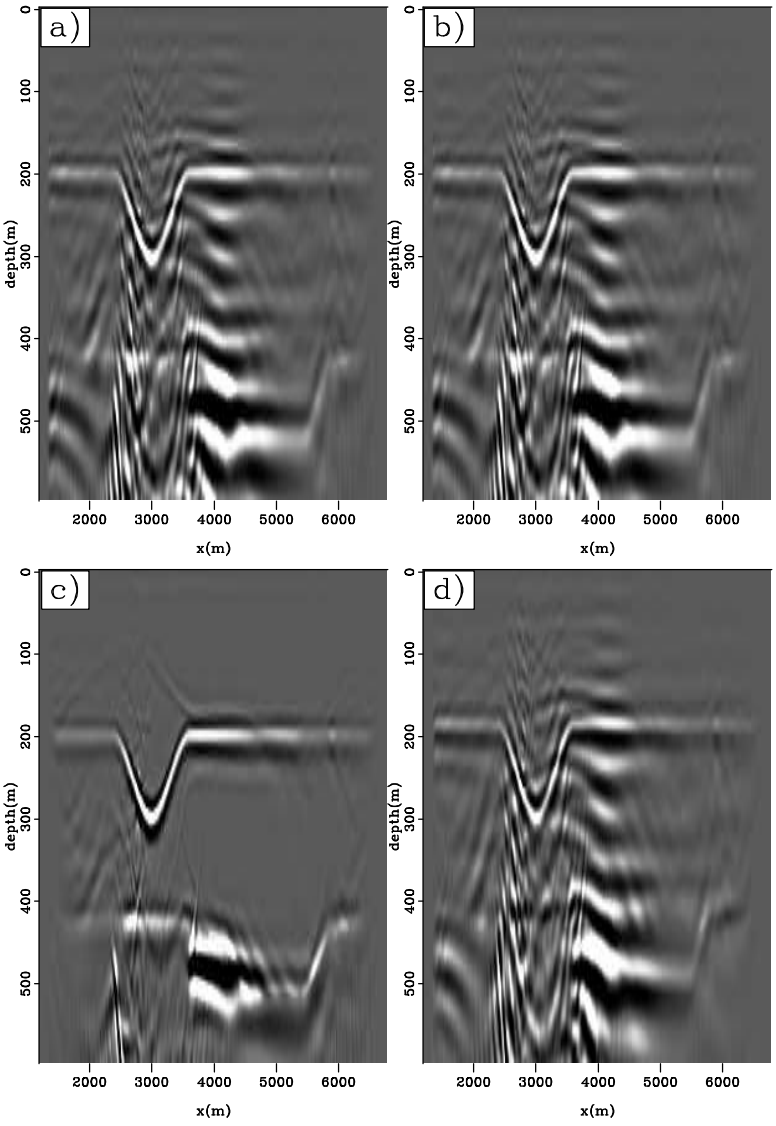

Figure 5.8: Top, left to right: Direct migration of two summed transmission wavefields without and with randomized source functions. c) Sum of images produced by direct migration of individual transmission wavefields. d) Horizontal plane-wave migration of the sum of correlations produced from the two wavefields, with randomized wavelets. DepthSyn-dmig1200.3500 [CR]

extended depth axis to show more of the deep artifacts. The second reflector stands out more clearly, and the multiple has been weakened in comparison to panel a. Two coherent cross-talk events have been introduced however. There is an event at $z = 300$ m and a mirrored event below the flat-bottomed syncline and many strange events in the deep image. These events are due to Fourier-domain wrap-around on the time axis. The time shift applied to the individual transmission wavefields associated with the application of the randomized wavelet often shifts late-time event around the time axis to early time. Energy at these times does not exist when the minimum traveltimes in each transmission wavefield is aligned. Since the source wavefield, D, is the same as the data wavefield, U, for direct migration, the algorithm images an inverted structure at deep depths when up- and down-going energy is propagated inappropriately (in opposite directions). The inverted structure is not exactly mirrored however, even though the time mirror would be symmetric. Convolution of the time records with the velocity model during migration leads to interesting combinations of the reflections with the velocity model.

Figure 5.9c shows the sum of the direct migrations of individual transmission wavefields. This result is very high quality and conforms the the requirement of independantly processing each transmission wavefield. Panel d shows the image produced by horizontal plane-wave migration of the gathers individually correlated, Figures 5.1a,b. This image suffers from steeply-dipping noise events, and the second layer shows weaker amplitude compared to the multiple reflection compared to the image c. They are otherwise roughly equivalent in quality.

Figure 5.10 presents direct comparissons between direct migration and the migration of synthesized gathers using modeled transmission wavefields below the entire domain. The top row of images was produced by independent processing of wavefields due to impulsive sources. The bottom row used a single transmission wavefield as input, which was produced by summing all the modeled wavefields due to randomized source functions. The left column images are direct migration results, and the right column images are migrations of synthesized shot gathers. Panel b is a reproduction of Figure 5.1c. Panels a and b are nearly indistinguishable. There are some minor amplitude differences and the migration of synthesized gathers, panel b seems to have a slightly broader wavelet. This minor difference could be caused by

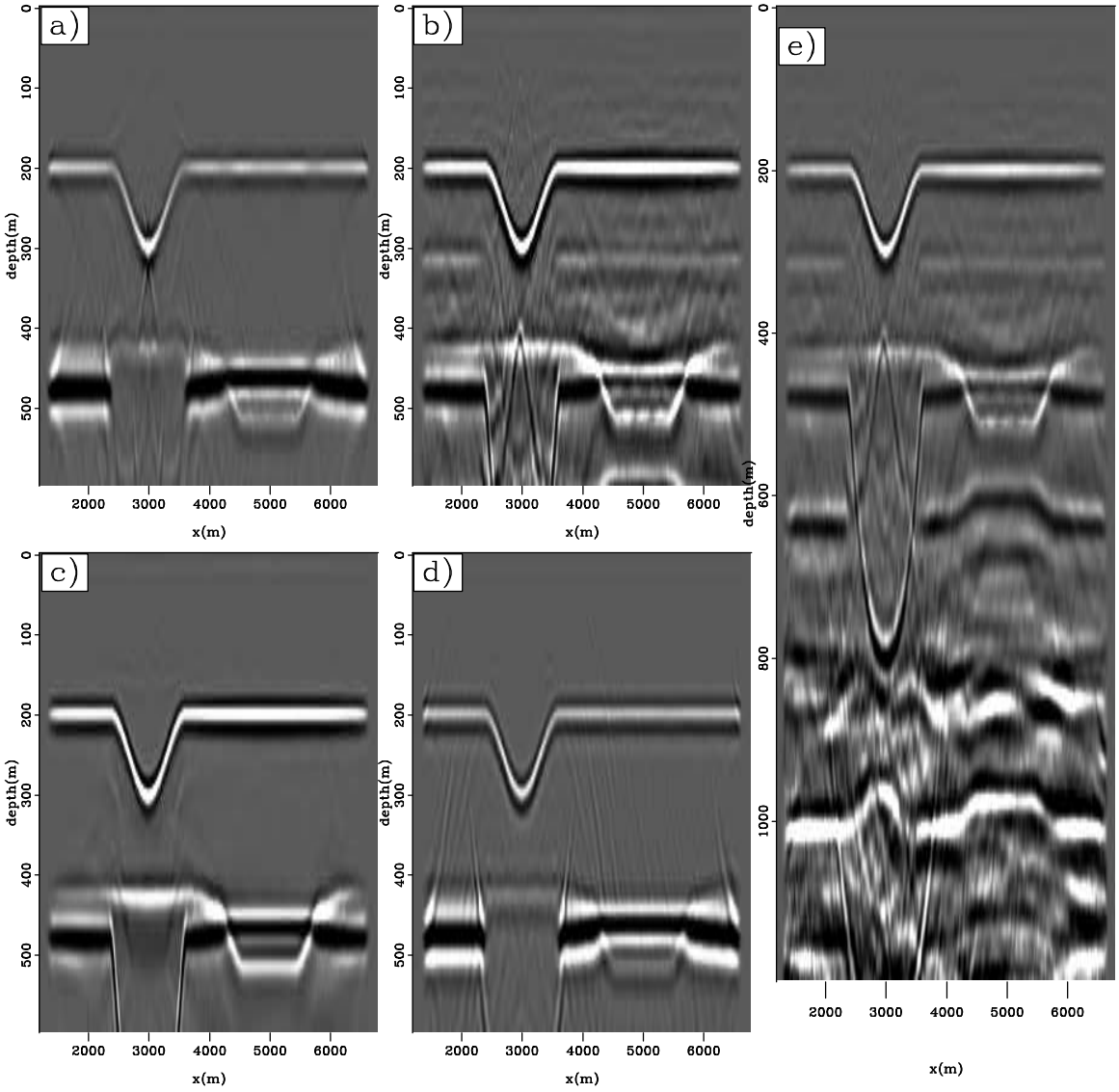

Figure 5.9: a) Direct migration of the transmission wavefield due to all 225 subsurface sources. b) Direct migration of summed transmission wavefields including randomized wavelets. e) Deep image using same data as image b. c) Sum of images produced by direct migration of individual transmission wavefields. d) Horizontal plane-wave migration of synthesized gathers produced by the sum of correlations from individual transmission wavefields. DepthSyn-dmigall [CR]

creating a source wavelet for use in the down-going wavefield, D, with slightly different characteristics than the wavelet resulting from the correlations. I used a standard Ricker wavelet for all migrations conforming to the conventional shot profile migration. The number of modeled transmission wavefields used to produce image `a` was the same as the number of virtual shots and receiver locations to produce image `b` which made the cost of the migrations roughly equivalent. However, synthesizing the gathers used as input for the migration to produce panel `b` requires substantial preprocessing that is not required for direct migration.

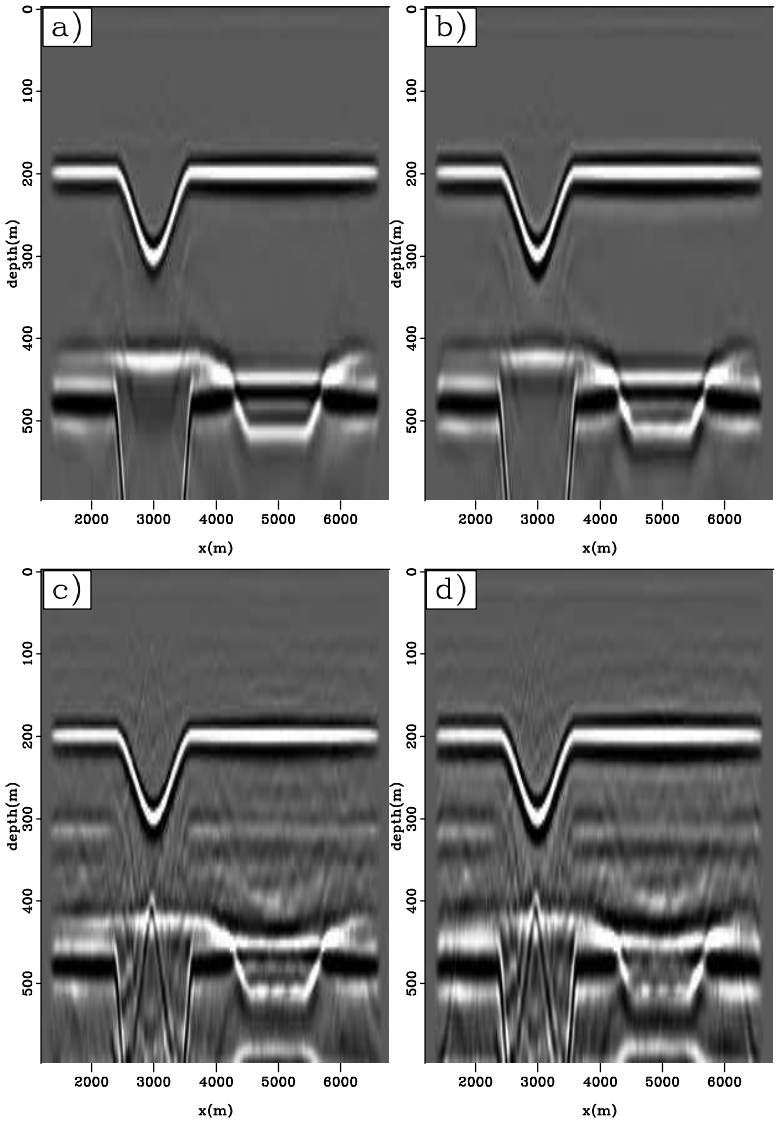

Figure 5.10: Left column shows direct migrations, while right column shows migrations of synthesized gathers. Top row processed impulsive transmission wavefields independantly, while the bottom row used a single transmission wavefield generated by summing the transmission wavefields due to randomized subsurface sources distributed densely below the entire model domain. DepthSyn-allcomp [CR]

Figures 5.10c and d compare direct migration (left) to the migration of synthesized gathers (right) when a single transmission wavefield due to subsurface sources below the entire domain. This experiments represents processing the passive data records from an entire data collection campaign simultaneously. The image in panel d took 123 minutes, while the direct migration image took only 0.41 minutes to produce: a cost ratio of 300. Again, the images are almost indistinguishable. All the main features in the image are directly comparable, though the events in the migration of correlations look to be of marginally lower frequency content.

Figure 5.11 shows images produced with the sum of transmission wavefields due to sources sparsely, but evenly distributed across the bottom of the model domain. The left column used wavefields with impulsive source functions, while the right column introduced randomness to the length, wavelet, and time delay of the source function. The top row was produced with direct migration, and the bottom row was produced with the horizontal plane-wave strategy beginning with synthesized shot gathers. The two plane-wave migrations are of very poor quality, though marginally interpretable. However, the implied dip of the shallow reflector in the left image is incorrect. The direct migrations produce a much better image. This is due to the sum of all the subsurface sources not creating a horizontal plane wave. Though sources were distributed across the entire domain, they were too far apart to generate a plane wave.

Figure 5.12 presents the top row of images from Figures 5.5 and 5.11 for comparison. The top row were produced by migrating the correlations (with and without randomized source functions) of the summed transmission wavefields. The bottom row was produced by direct migration. The images are very comparable. There is a minor phase roll between the two processing versions. The second reflector is marginally more continuous and less effected by noise in the direct migration.

Figure 5.13 shows images produced with the sum of transmission wavefields due to 30 sources clustered around the center of the model domain. The left column used wavefields with impulsive source functions, while the right column introduced randomness to the length, wavelet, and time delay to the source function. The top row was produced with direct migration, and the bottom row was produced with the horizontal plane-wave strategy beginning with synthesized shot gathers using the summed transmission wavefield. The two direct migration images are very comparable. Again, steep, coherent noise on the left is eliminated with the

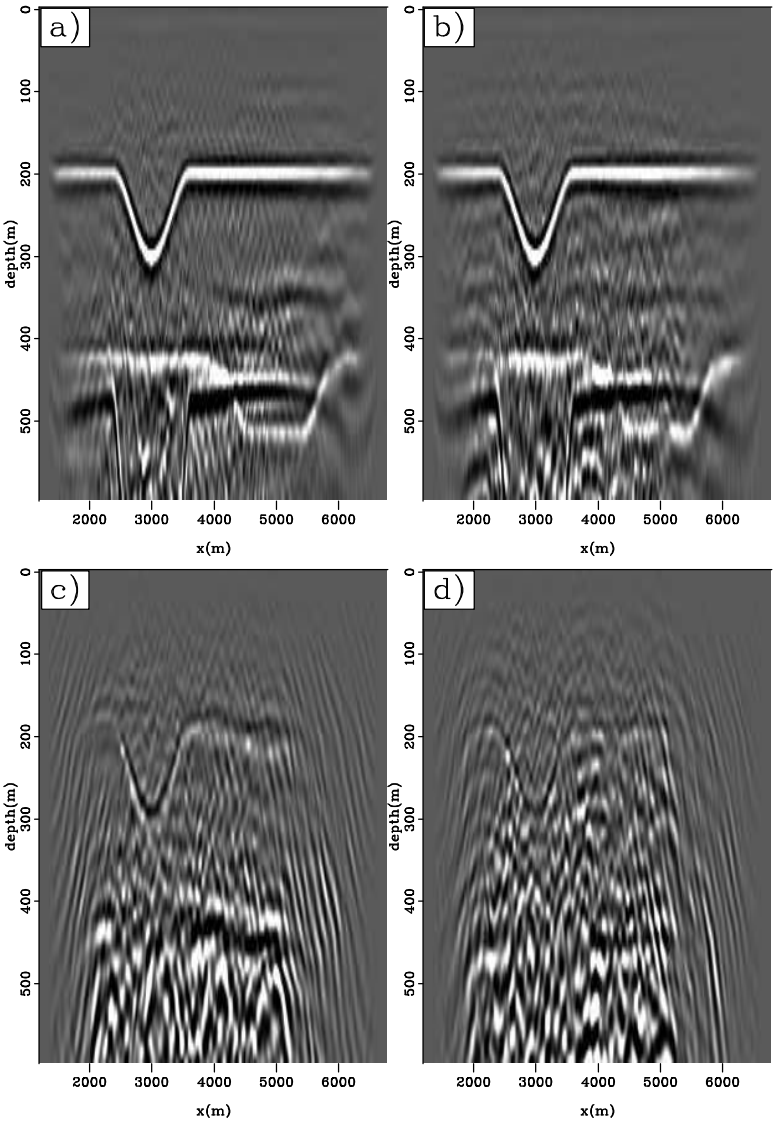

Figure 5.11: Images produced from a transmission wavefield due 30 source clustered around the center of the bottom of the model domain. Top row was produced by direct migration. Bottom row was produced by horizontal plane-wave migration of the correlated gathers produced with the transmission wavefields used for direct migration above. Left column used impulsive source functions, while the right column used randomized source functions. DepthSyn-dmigsmall [CR]

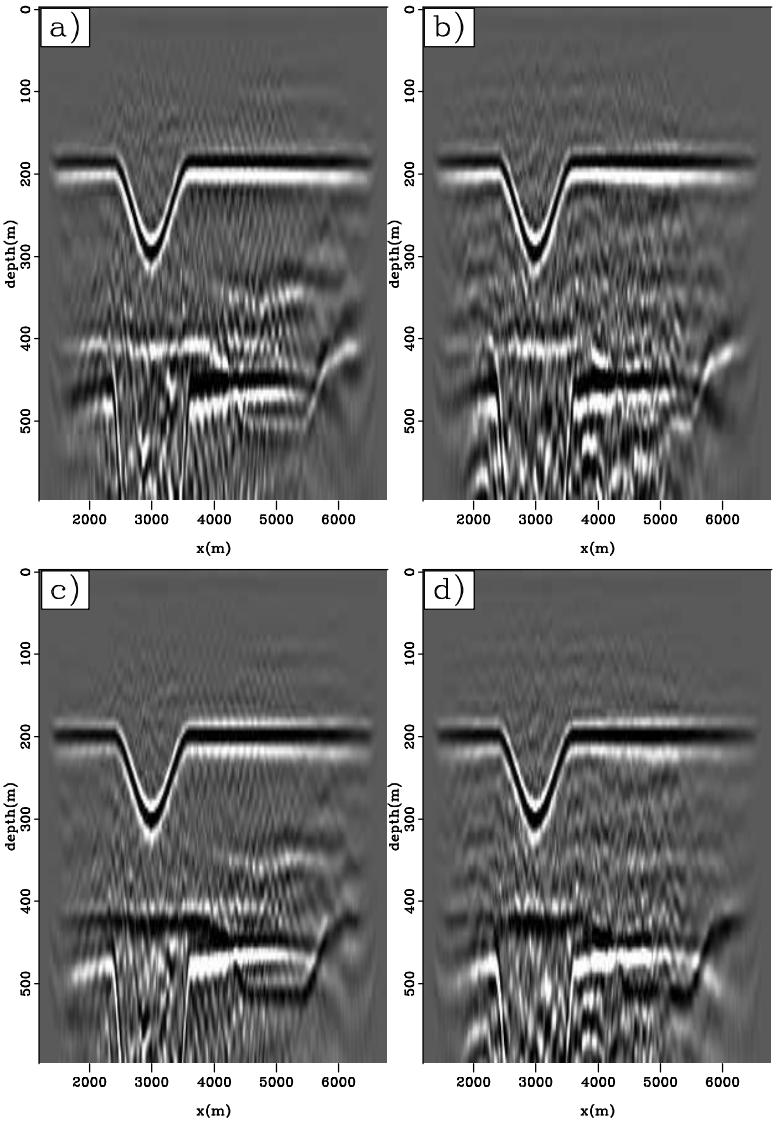

Figure 5.12: Comparison of processing strategies to image a transmission wavefield due to 25 sources distributed evenly across the bottom of the domain. Top: Migration of correlations. Bottom: Direct migration of the wavefield. Left column summed wavefields as modeled, while right column convolved each wavefield with a random wavelet before summing. DepthSyn-smallcomp [CR]

introduction of randomness, while the coherence of the structure suffers marginally. The bottom row is also a poor result when the limited areal distribution of subsurface sources can not synthesize a plane wave during summation.

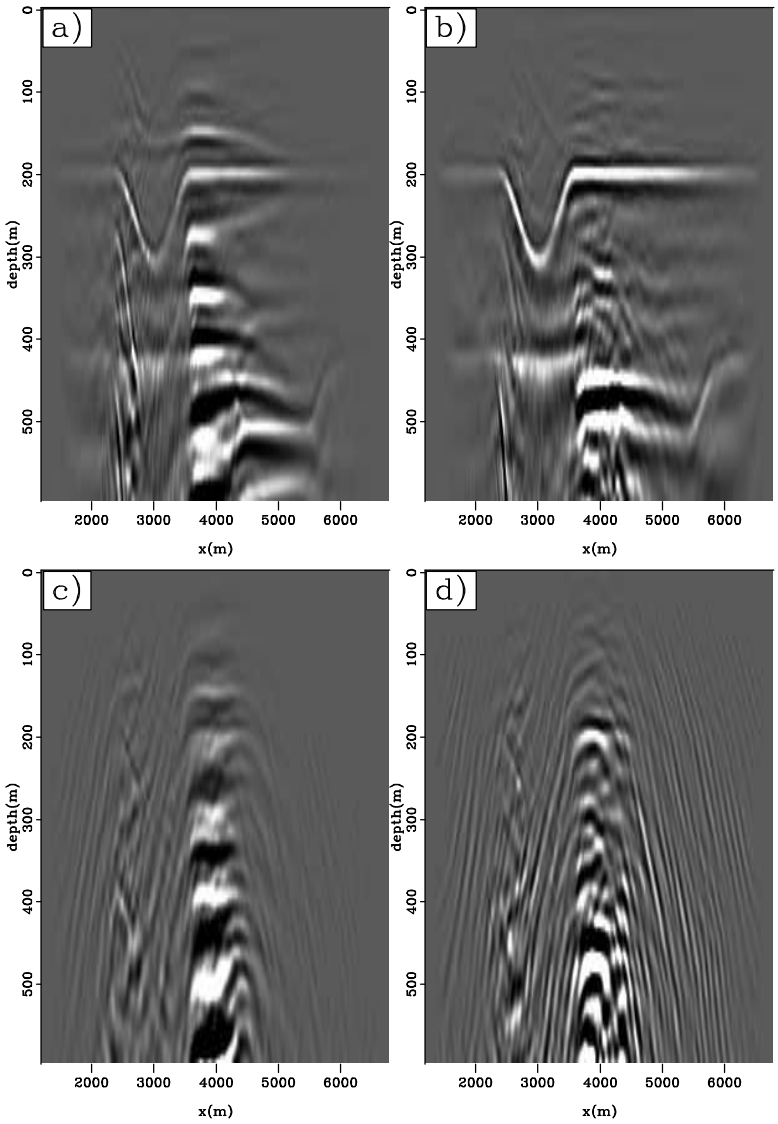

Figure 5.13: Images using summed transmission wavefields due to 30 sources clustered around the center of the model domain. Top row, left to right: Direct migration with impulsive sources and randomized sources. Bottom row, left to right: Horizontal plane-wave migration using synthesized gathers without and with randomized source functions. DepthSyn-dmigsmallsmall [CR]

Figure 5.14 presents the bottom row of images from Figure 5.5 and the top row of Figure 5.13 for comparison. The summed transmission wavefield used for these images was the result of 30 subsurface sources below the center of the model domain. The results including randomized wavelets are in the right column. These images roughly reinforce the observations made above. The migration of correlations (top row) are marginally poorer at a very fine level

of detail. The direct migration strategy does a little better imaging the second reflector. However, the two techniques produce largely equivalent images with only a minor phase difference in the wavelets with which the reflectors are convolved.

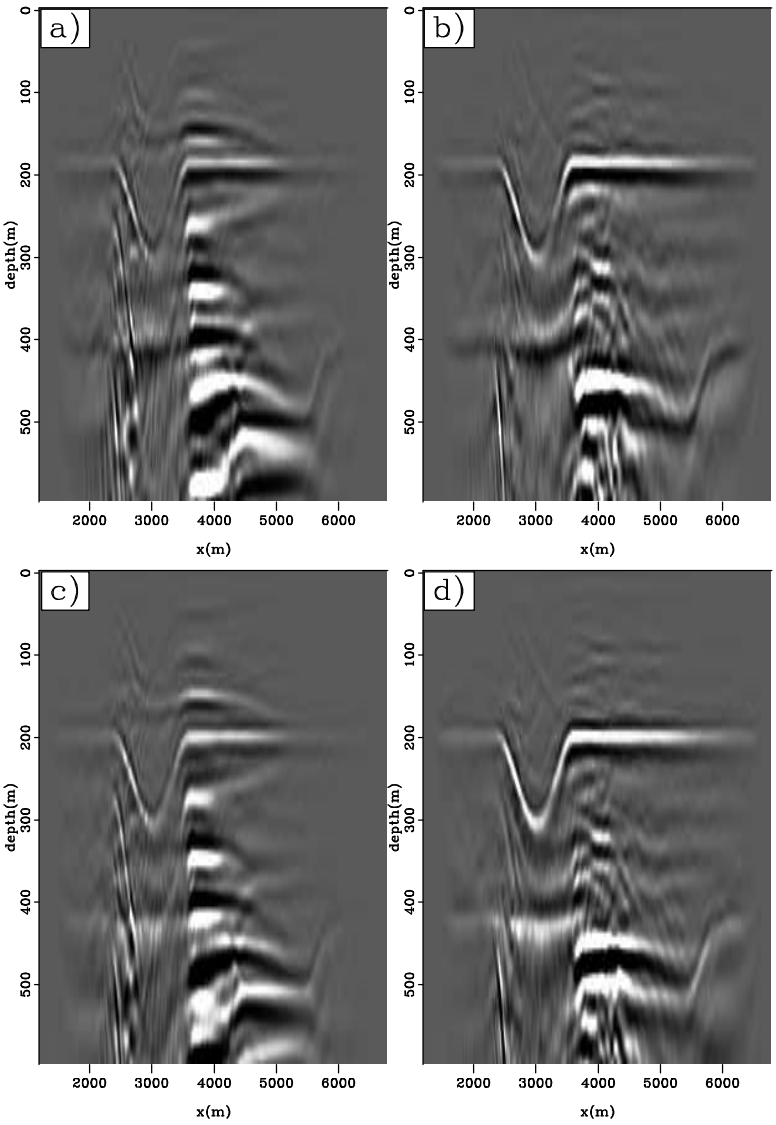

Figure 5.14: Comparison of processing strategies to image a transmission wavefield due to 25 sources distributed evenly across the bottom of the domain. Top: Migration of correlations. Bottom: Direct migration of the wavefield. Left column summed wavefields as modeled, while right column convolved each wavefield with a random wavelet before summing. DepthSyn-smallsmallcomp [CR]

CONCLUSIONS

Migration is a powerful operator that substantially reduces the complexity and size of the volume of data to be analyzed and often diminishes noise in the input data volume, or transforms it to an obvious character. Transmission wavefields are inherently imperfect data volumes compared to those produced with active seismic experiments. Migration greatly simplifies the complexity and volume of data to interpret, provided a reasonably accurate velocity model is available. While this could be a potential disadvantage, the expense related with mounting a passive recording campaign will, for the near future, limit passive acquisition to fairly well understood areas where a good velocity model has already been generated. If not, a reasonable initial model can be constructed and then refined through iterative methods.

Using transmission wavefields modeled only across the bottom of a subsurface domain, the rigorous equation to synthesize the conventional active seismic data volume is not obeyed. Even though coherent noise events remain in the synthesized gathers, the migrated images do not suffer substantially from their presence. When multiple sources are captured in a transmission wavefield during the recording of a passive seismic experiment, the cross-talk associated with correlation can lead to misinterpreting the shot gathers. This misinterpretation of the subsurface is minimized, though not mitigated completely, by migration.

Correlation removes a round trip from depth to the surface. Therefore, the direct arrival is the appropriate source function to images the the first-order multiples. Similarly, the first-order multiples correctly image the subsurface structure as the source energy for second-order multiples, and so on. If high-order multiples are recorded in the transmission wavefield, these events contribute to correct imaging at surface recording stations far away from the horizontal location of the subsurface source. If the sources are weak, and attenuation of the energy does not allow recording high-order multiple reflections from the reflectors at depth, synthesized shot gathers and direct migration images will not image structure at large horizontal distance from the subsurface source.

For a transmission wavefield due to many subsurface sources distributed completely across the model domain, the source energy sums to vertically propagating plane wave. In this case,

wavefront imaging (direct migration) provides an almost equivalent image to horizontal plane-wave imaging. If the number of subsurface sources is small, or the distribution has large gaps, the sum of the direct arrivals does not produce a horizontal plane wave and processing the synthesized gathers under this assumption is inappropriate.

Rather than framing the correlation processing of transmission wavefields as an interferometric calculation of Green's functions, I believe that analyzing the use of transmission data as an imaging problem provides an intuitive and simple framework: direct migration. The experiments presented above show that processing transmission wavefields as an imaging problem within the framework of shot profile depth migration is a valid strategy akin to phase-encoded migration or a repeated datuming excersize. The images created by correlation followed by migration are very similar to those created by direct migration. Therefore, correlation and extrapolation are commutable operators and we are free to choose a strategy most convenient for the task, or data, at hand. If passive data are available from an area with no knowledge of the subsurface velocity field, it may be neccessary to correlate the records before migration. However, even if the synthesized gathers seem to show little or no correct information about the subsurface, migrating the data may provide surprisingly good results.

If a velocity model is available, and migrating the data is a foregone decision, direct migration can save substantial computational cost. Because depth migration is an expensive operation, minimizing the volume of input data can drastically effect the total cost to process a data set. Correlating every trace with every other trace squares the data volume. Therefore, if the raw data can be windowed into fewer transmission wavefields than the number of deployed receivers, it is always less expensive to migrate the raw data. Also, direct migration does not require an inverse Fourier transform of the large volume of synthesized gathers. It is possible to skip the inverse transform and input the gathers directly into a mixed-domain migration algorithm. However, after showing that the two processing algorithms produce roughly equivalent results, it seems a waste of computer time to compute the gathers and not view them in the time domain. After computing synthesized gathers, it may be advantageous to attempt noise removal or address aliasing problems. However, because gathers synthesized with an incomplete number and/or distribution of subsurface source do not perfectly recapitulate active surface seismic data, such efforts may be difficult or result in removal of events that are useful

to imaging the subsurface during migration.